Crystal structure and surface relaxation in Cr_2O_3 with a transferable oxide interaction potential

1999 J. Phys.: Condens. Matter 11 1903

(http://iopscience.iop.org/0953-8984/11/8/004)

J. Phys.: Condens. Matter **11** (1999) 1903–1914. Printed in the UK PII: S0953-8984(99)99619-4

Crystal structure and surface relaxation in Cr_2O_3 with a transferable oxide interaction potential

Adrian J Rowley, Mark Wilson and Paul A Madden

Physical and Theoretical Chemistry Laboratory, University of Oxford, South Parks Road, Oxford OX1 3QZ, UK

Received 24 November 1999

Abstract. An extended ionic interaction model, originally devised for alkaline earth oxides, is transformed into a potential for Cr_2O_3 by scaling parameters in a well-defined way to allow for the changes in cation radius and charge and in ionic polarizability. The extended ionic model allows for the induction of dipoles and quadrupoles and for deformations in the ionic shape, as perceived through the short-range interionic repulsion. The transformed potential predicts corundum as the lowest energy crystal, as is observed experimentally: induced quadrupoles are confirmed as playing an important role in stabilizing this structure. The predicted unit cell parameters and ionic positions are in good agreement with experiment. The model is used to study the relaxation of two low index surfaces, (0001) and $(01\bar{1}2)$. The $(01\bar{1}2)$ is shown to be energetically favoured over the (0001), which is consistent with the experimental observation of it as a free surface. The relaxation of the (0001) surface is shown to be in excellent agreement with LEED observations and with *ab initio* studies, in which several layers of ions are allowed to fully relax.

1. Introduction

Despite the advent of *ab initio* simulation methods [1, 2], the development of transferable ionic interaction models remains a holy grail of materials modelling [3]. Such potentials are far cheaper to evaluate and permit the use of large simulation cells and long runs, which is often desirable. Also, for a complete interaction model, the parameters should vary in a physically (chemically) meaningful way from one material to another. The potentials then give insight into the underlying factors responsible for the specific properties of materials. Such a complete potential developed for one material could be 'transmuted' into that for another, or used to describe the relevant interactions in mixtures, i.e. it would be transferable. In the present work, we examine the completeness of a description of the interactions of an oxide ion in MgO and CaO [4, 13] by transforming their parameters in a physically meaningful way to obtain a potential for Cr_2O_3. We then examine the surface properties of the Cr_2O_3 crystal, which are of interest due to its use as an industrial catalyst in the manufacture of CFC replacements [5, 6, 7].

In our terms [8], an ionic interaction potential represents the possible interactions between closed-shell ions carrying formal charges. Such interactions are not fully represented by the pair potentials which have traditionally been regarded as ionic models. Instead, many-body effects may arise from the deformation of an ion (particularly the anion) by both short-range and coulombic interactions with other ions. These effects are represented in extended ionic models, such as the shell model [9], but shell models have been beset by difficulties of parameterization, which have jeopardized their transferability. Systems of stoichiometry M_2O_3 (M, trivalent metal cation; O, oxide anion) represent a stern test of such ionic potentials. Compounds of MO

0953-8984/99/081903+12$19.50

or MO_2 stoichiometries often have relatively simple (small unit cell, high symmetry) crystal structures whose formation may often be understood in terms of sphere packing arguments (essentially radius-ratio rules). The M_2O_3 stoichiometry is more complex in that the greater variety of packing options leads to lower symmetry structures often with relatively large unit cells. As a result, although the short-range order (the nearest-neighbour anion–cation coordination shell) may often be understood in terms of the same radius-ratio arguments, the overall low symmetry may lead to other factors, such as polarization effects, which play a significant role in determining the ground state crystal structures. Unless a potential can describe the near-spherical oxide ion, relevant to the high symmetry MO crystals as well as the deformed ion, which will exist even in the equilibrium crystal structure in M_2O_3, it will not transfer between these stoichiometries [10].

Nevertheless, the cubic MO crystals provide a very good starting point for the construction of oxide potentials: the small unit cell and high symmetry mean that *ab initio* electronic structure calculations can be used to study unambiguously the response of the oxide ion to changes in its immediate environment. In this way, a systematic examination of the origin of many-body effects may be undertaken. This has shown the importance of the spherical compression of the oxide ion by surrounding cations in the selection of the preferred coordination number [11, 12] and has clarified the contribution of dipolar and quadrupolar polarization effects to the energetics of the distorted crystals, as sampled by particular phonons [4]. The incomplete description of the interactions, which includes only the spherical compression and polarization effects, is highlighted by a comparison between predicted and observed phonon frequencies. The remaining effects, necessary to achieve a complete description of the phonons in MgO, are due to changes in shape of the oxide ions, as perceived in the short-range repulsive interactions ('aspherical ion model', AIM, effects). The parameters which appear in this interaction model represent physically meaningful quantities such as ion radii, polarizabilities etc, and should transform predictably from one oxide compound to another. This expectation can be directly checked by comparison with further *ab initio* and experimental data for CaO and SrO [13], and leads to proposed procedures for scaling potential parameters, which we exploit in section 2, to propose a potential for Cr_2O_3. In M_2O_3 systems there are no comparable highly symmetric structures on which to base a comprehensive parameterization strategy.

For Cr_2O_3 in the experimentally observed corundum structure, the Cr^{3+} ions occupy two-thirds of the available octahedral holes in a hexagonally close-packed anion sublattice. The partial occupancy of these holes leads to a filled-filled-unfilled pattern in the direction of the *c*-axis. As a result, the cations are pushed towards one side of the hole since the coulombic cation–cation repulsion between a pair of nearest-neighbour cations (in the *c*-direction) is not counterbalanced because the next site along is a hole [14]. The distortion means that there are two characteristic anion–cation nearest-neighbour separations in the ideal crystal. However, whilst the corundum structure is the experimentally observed ground state, simple ionic (shell) models predict the alternative bixbyite structure [15]. This structure is also based on six-coordinate cations and can be thought of as formed from a fluorite (CaF_2) structure in which one quarter of the anions have been removed. As a result, although the cations are actually six-coordinate, they can be thought of as sitting in a 'pseudo-eight-coordinate' hole. This is reflected in the fact that these structures are favoured by larger cation M_2O_3 systems. In previous work focusing on corundum (Al_2O_3) itself, it was shown how the inclusion of induced quadrupoles on the oxide ions was crucial in stabilizing the corundum structure over the bixbyite [14]. The induced quadrupoles in the corundum structure are significantly larger than in the bixbyite, since the four-coordinate cation shell about each anion is more distorted from a tetrahedral configuration towards a square planar arrangement. Thus, the relatively

low crystal symmetry leads to the induced anion quadrupoles playing a significant role in determining the ground state crystal properties.

Therefore the interplay between ion size effects and polarization and aspherical deformation is already apparent in the energetics of possible crystals, which thus represents a significant challenge for our 'transmuted' interaction potential, as discussed in section 3. There we shall study two low index surfaces, where the ions are in highly asymmetric environments and where ion deformations and polarization effects would be expected to play an even more significant role than in the bulk crystal. The internal strains within the corundum crystal, due to the asymmetric pattern of hole occupancy, mean that the surfaces can often undergo relatively large relaxations when the cleavage leads to subtle balancing factors being removed.

The surfaces chosen for the present study are the cation terminated (0001) basal plane, as it is relatively simple, has been studied *ab initio* both for Cr_2O_3 [16] and Al_2O_3 [1, 2] and has recently been the subject of LEED experiments [17], and the $(01\bar{1}2)$ surface which has also been studied *ab initio* [18]. The relative energies of these two surfaces are the subject of some controversy. X-ray diffraction [19] and electron microscopy studies [20] show the latter to be energetically favourable. Indeed, although Al_2O_3 and Cr_2O_3 do not readily cleave, both Ti_2O_3 and V_2O_3 do cleave along the $(01\bar{1}2)$ plane [21, 22, 23]. Additionally, there is a possible high pressure transition to a Rh_2O_3-II structure which can be thought of as a series of $(01\bar{1}2)$ grain boundaries [24, 25, 26].

2. Model

The many-body aspects of the interactions reside in both the short-range repulsion and the polarization parts of the potential. In addition, the potential contains pair potentials for dispersion interactions and the charge–charge coulomb interactions. Formal charges of +3 and -2 are used for the Cr and O ions, respectively. We neglect polarization of the cation and treat the short-range repulsion between a pair of oxide ions with exactly the same potential as used to describe the alkaline earth oxides. Hence, the most important effects which we must allow for, in transmuting our MO potential to Cr_2O_3, are the effects of the change of cation on the short-range repulsion between cation and anion and on the polarization terms. The cation radii of Cr^{3+} is $\sigma_{Cr^{3+}} = 0.64$ Å compared to values of $\sigma_{Ca^{2+}} = 1.06$ Å for Ca^{2+} [27]. We will pursue the parameterization of the potential in some detail to emphasize the fact that the only quantities which enter the parameter-scaling are the cation radius and the dipole and quadrupole polarizabilities of the oxide ion in the crystal.

2.1. Polarization and dispersion terms

We have discussed the transformation of the anion polarization terms between systems with different cations in several papers dealing with halide systems [8, 28]. The change of cation may alter the value of the ion polarizabilities, which is an important effect for oxides [29], and may also change the short-range damping parameters (srdp) [8] which determine the length scale over which short-range cation–anion interactions induce dipoles and quadrupoles. In the alkaline earth systems, both types of parameter have been examined *ab initio* [30].

For Cr_2O_3, estimates of the anion and cation dipole polarizabilities are obtained from experimental refractive indices for CrF_3 (1.57 [31]) and Cr_2O_3 (2.55 [31]) via the Clausius–Mossotti relationship, under the assumptions [32] that the Cr^{3+} polarizability will be the same in both crystals and that the F^- polarizability has the same value as in LiF ($\alpha_{F^-} = 6.2$ [33]). This leads to $\alpha_{Cr^{3+}} = 6.7$ a.u. and $\alpha_{O^{2-}} = 12.4$ a.u.. The latter value seems reasonable compared with a value of 16.2 a.u. in CaO [32] and 11.3 a.u. in MgO [32], which falls to 9.2

a.u. in Al_2O_3 [14].

The construction of the quadrupolar portion of the polarization model represents more of a challenge. We require a quadrupole polarizability, C, and dipole–dipole–quadrupole hyperpolarizability, B. To obtain a value for C, we interpolate in terms of cation radii between the *ab initio* values of 26 a.u. and 33 a.u. for the O^{2-} ion in MgO [34] and CaO [35] respectively, giving a value of 29.6 a.u.. The approximation $B \simeq -6\,C$, which approximately describes the relationship between the polarizabilities in cases where they have been studied, gives a value of −178 a.u. for B.

The short-range damping effect is included in the polarization interactions by modifying the radial form of the charge–dipole and charge–quadrupole interactions with a Tang–Toennies function [36],

$$f_{n_k}(r^{ij}) = 1 - a\mathrm{e}^{-br^{ij}} \sum_{k=0}^{n_k} \frac{(br^{ij})^k}{k!}. \tag{1}$$

The parameter b is the srdp (b_2 and b_3 for the dipolar and quadrupolar terms respectively [4]) and represents the range over which the short-range effects act. For induction damping, we normally use $n_k = 4$. The parameter a is the amplitude of the short-range interaction. a and b have been investigated in *ab initio* calculations on the alkaline earth oxides [30], where values of $a = 1$ and $a = 2$ are used for dipole and quadrupole damping respectively, and where the values of b are found to scale with the sum of cation and anion radii. We therefore keep a values as above and find b values for Cr_2O_3 from those for CaO by the scaling

$$b_{Cr_2O_3} = b_{CaO} \frac{\sigma_{Cr^{3+}} + \sigma_{O^{2-}}}{\sigma_{Ca^{2+}} + \sigma_{O^{2-}}}. \tag{2}$$

The induction damping terms acting between pairs of oxide anions are omitted for simplicity since these terms only manifest themselves very subtly in, for example, phonon modes [4]. The full set of polarization parameters is given in table 1.

Table 1. Cr_2O_3 polarization parameters. $\alpha_{O^{2-}}$, $C_{O^{2-}}$ and $B_{O^{2-}}$ are the dipole, quadrupole and dipole–dipole–quadrupole (hyper)polarizabilities respectively. b_2 and b_3 and the dipole and quadrupole damping parameters follow the nomenclature of [4].

Parameter	Value (a.u.)	Parameter	Value (a.u.)
$\alpha_{O^{2-}}$	12.4	b_2	1.32
$C_{O^{2-}}$	29.6	b_3	1.50
$B_{O^{2-}}$	−178.0		

The polarizabilities given above and the electron numbers from [32] may be used to estimate the dipole–dipole and dipole–quadrupole dispersion terms

$$V_{disp} = \frac{1}{2} \sum_{i,j} \frac{C_6^{ij}}{(r^{ij})^6} f_6(r^{ij}) + \frac{C_8^{ij}}{(r^{ij})^8} f_8(r^{ij}) \tag{3}$$

using the Slater–Kirkwood [37] and Starkschall–Gordon formulae [38] respectively. The dispersion damping is again represented through a Tang–Toennies function with the range parameter for the cation–anion interactions scaled from CaO by the ratio of ionic radii, as above. The dispersion parameters are given in table 2.

Table 2. Cr_2O_3 dispersion parameters. All values are in a.u.. The damping parameters are for $n_k = 6$ and 8 in equation (1) for the dipole–dipole and dipole–quadrupole damping respectively.

Ion-pair	C_6	b	C_8	b
O–O	69.1	1.85	1292	2.0
Cr–O	45.9	1.83	0.0	—
Cr–Cr	30.0	—	0.0	—

2.2. The short-range interaction

As discussed in [4] the short-range cation–anion repulsive potential allows for changes in the size and shape of the anion

$$V_{sr}(\{\mathbf{r}_i, \delta\sigma_i, \boldsymbol{\nu}_i, \boldsymbol{\kappa}_i\}_{i=1,N}) = \tfrac{1}{2}\sum_{i\in anion}\sum_{j\in cation} f_{-+}(r_{ij}, \delta\sigma_i, \boldsymbol{\nu}_i, \boldsymbol{\kappa}_i) + \sum_{i\in anion} v_{self}(\delta\sigma_i, \boldsymbol{\nu}_i, \boldsymbol{\kappa}_i) \quad (4)$$

where $\{\delta\sigma_i, \boldsymbol{\nu}_i, \boldsymbol{\kappa}_i\}_{i=1,N_{anion}}$ are dynamical variables which represent changes in the anion shape of spherical, dipolar and quadrupolar symmetry, respectively. At each ionic configuration the energy in (4) is minimized with respect to these variables, so that, in molecular dynamics, they follow the ion motion adiabatically. The first term in (4) is a pair interaction potential and the second is a 'self-energy' which gives the energy cost for an anion to reach the state of deformation described by $\delta\sigma_i$, $\boldsymbol{\nu}_i$ and $\boldsymbol{\kappa}_i$. f_{-+} is typically of the form

$$\begin{aligned} f_{-+}(r_{ij},\ \delta\sigma_i,\ \boldsymbol{\nu}_i,\ \boldsymbol{\kappa}_i) = {} & A_{-+}e^{-a_{-+}(r_{ij}-(\bar{\sigma}_i+\delta\sigma_i)-(\bar{\sigma}_j)-\mathbf{S}^{(1)}(\mathbf{r}_{ij})\cdot\boldsymbol{\nu}_i-\mathbf{S}^{(2)}(\mathbf{r}_{ij})\cdot\boldsymbol{\kappa}_i)} \\ & + B_{-+}e^{-2a_{-+}(r_{ij}-(\bar{\sigma}_i+\delta\sigma_i)-(\bar{\sigma}_j)-\mathbf{S}^{(1)}(\mathbf{r}_{ij})\cdot\boldsymbol{\nu}_i-\mathbf{S}^{(2)}(\mathbf{r}_{ij})\cdot\boldsymbol{\kappa}_i)} \end{aligned} \quad (5)$$

where $S^{(1)}_\alpha(\mathbf{r}) = r_\alpha/r$ and $S^{(2)}_{\alpha\beta}(\mathbf{r}) = 3r_\alpha r_\beta/r^2 - \delta_{\alpha\beta}$. This contains three parameters A_{-+}, B_{-+} and a_{-+}, which set the amplitude and range of the pair term, together with mean radii $\bar{\sigma}_i$ and $\bar{\sigma}_j$ for the anion and cation. To transform this part of the short-range potential from CaO to Cr_2O_3 the only parameter which is altered is the cation radius. The self-energy is written as a sum of terms in each of the deformation variables

$$v_{self}(\delta\sigma_i, \boldsymbol{\nu}_i, \boldsymbol{\kappa}_i) = D(e^{\beta\delta\sigma_i} + e^{-\beta\delta\sigma_i}) + (e^{\xi^2|\boldsymbol{\nu}^i|^2} - 1) + (e^{\eta^2|\boldsymbol{\kappa}^i|^2} - 1) \quad (6)$$

where each of these functions is quadratic (harmonic) in the deformation variables $\delta\sigma_i$, $\boldsymbol{\nu}_i$ and $\boldsymbol{\kappa}_i$ about their undeformed values ($\delta\sigma_i = 0$ etc), so that β, ξ and η are force constants which resist the deformation. In the undeformed state, v_{self} takes the value $2D$ which is a measure of the electron affinity of the O^- ion in the material [39]. For Cr_2O_3 we use the *ab initio* determined values for D and β in CaO. In the alkaline earth oxide work, we noted that ξ and η scaled as the reciprocal of the dipole and quadrupole polarizability of the oxide ion, and we therefore scale the CaO values to Cr_2O_3 using the above-mentioned polarizabilities.

Full details of the parameters for the short-range cation–anion potential are given in table 3. In the following section, we dub this potential the AIM (aspherical ion model). We will

Table 3. Parameters of the short-range cation–anion interaction (equations (5) and (6)) in atomic units. The atomic unit of energy is the Hartree = 2625 kJ mol^{-1}, and that of length the bohr = 0.52918Å.

Parameter	Value	Parameter	Value
a_{-+}	1.718	ξ	0.54
A_{-+}	55.24	η	2.00
B_{-+}	2.68×10^4		

contrast its properties with simpler potentials obtained by ignoring some of the many-body effects already described. In particular, we will consider the dipolar AIM, where quadrupole induction and quadrupole ion deformation are ignored. We will also describe results for the CIM (compressible ion model) in which all aspherical deformation and induction effects are neglected i.e., the only remaining many-body effect is the spherical breathing of the anions.

3. Crystal structures

As discussed in the introduction, the two most likely crystal structures are bixbyite and corundum [14, 15]. The crystal energy minima are located at each volume (and c/a ratio for the corundum) by allowing the ion positions to evolve under molecular dynamics equations of motion and by periodically removing the kinetic energy (essentially a simulated annealing method).

Table 4. Cr_2O_3 lattice parameters (a.u.), energies (kJ mol^{-1}) and molar volumes (cm^3). Experimental values are from [40].

Parameter	Full model	Dipolar model	CIM	Expt.	HF[16]	Al_2O_3 expt. [41]
a_0	9.45	9.55	9.60	9.37	9.52	8.99
c_0	25.23	25.50	25.44	25.7	25.93	24.55
c/a	2.67	2.67	2.65	2.74	2.72	2.73
u	0.3554	0.3555	0.3540	0.3475	—	0.352
v	0.286	0.284	0.292	0.306	—	0.306
Lattice energy	−12946	−12834	−12818	−12823	—	—
Molar volume	29.03	29.96	30.20	29.17	30.29	25.57
ΔU	−10	+ 30	—	—	—	—

Figure 1 shows the energy/volume curves for the full AIM potential, as described in the previous section. The energy of the corundum structure is minimized with respect to the lattice constants and u_{Al} and u_O, which describe the positions of the aluminium and oxide ions within the unit cell. The bixbyite minimizations are simpler since, the system being cubic, these only have to be minimized with respect to the single lattice parameter and the internal coordinates. Table 4 summarizes the crystal properties for the corundum minimum compared with experiment and Hartree–Fock (HF) calculations [16]. The agreement with experiment is excellent. We recall that the model has been obtained by scaling potentials derived for other oxide materials without reference to this crystal structure or, in fact, to this stoichiometry at all. The largest error observed is in u_O, which indicates that the oxide sublattice is more distorted from the ideal hexagonal close-packed arrangement than is observed experimentally. The bixbyite structure is at a higher energy than the corundum and has a higher equilibrium molar volume reflecting the 'pseudo-eight-coordinate' nature of this structure. Table 4 also lists the minimized corundum crystal structure parameters for two different levels of the model; the CIM (spherical anion relaxation only) and the dipolar AIM (ion distortions and polarization effects included to a dipolar level only). The addition of these terms, which allow for aspherical deformation of the oxide ion in a low symmetry site, reduces the molar volume and increases the binding energy (reflected in the lattice energies). The internal parameters are also slightly affected, with the c/a ratio increasing as the quadrupolar effects are added.

Most importantly, the full AIM predicts the corundum to be energetically favoured over the bixbyite by $\simeq 10$ kJ mol^{-1}. In the absence of the quadrupolar terms (both polarization and

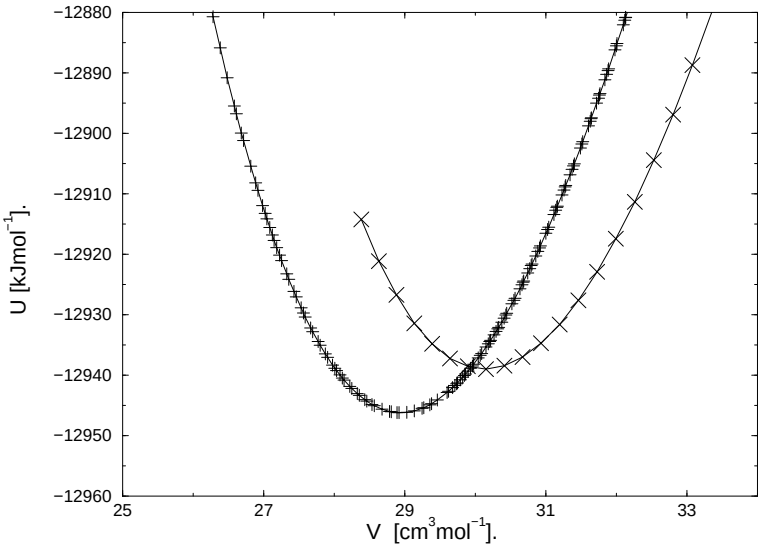

Figure 1. Internal energy versus volume curves calculated with the full AIM potential for Cr_2O_3 in its corundum (+) and bixbyite (×) modifications. For corundum each point is minimized with respect to the c/a ratio, u_O and u_{Al} as discussed in the text. Bixbyite is cubic and so is minimized with respect to a single lattice parameter and the internal coordinates.

AIM) the bixbyite is favoured over the corundum by $\simeq 30$ kJ mol^{-1}. The energy difference of $\simeq 10$ kJ mol^{-1} in the full AIM is smaller than the value of -76 kJ mol^{-1} calculated for Al_2O_3 using density-functional methods [14]. That this energy gap should be reduced on going to Cr_2O_3 from Al_2O_3 is consistent with simple cation size arguments. As already mentioned in the introduction, the bixbyite structure can be considered as formed from the fluorite in which the cations are eight-coordinate. As a result, the six-coordinate hole available in this structure can accommodate larger cations than can the truly octahedral hole in the corundum structure. A survey of the cations which form M_2O_3 crystals [42] shows that the ions from Al^{3+} to V^{3+} (radii 0.50 Å and 0.74 Å respectively) form corundum structures, whilst those from Sc^{3+} to Tl^{3+} (radii 0.81 Å to 0.95 Å) favour the bixbyite. As a result, the energy difference between these structures must change sign at a cation radius of about 0.76 Å. The energy difference of -76 kJ mol^{-1} represents an extreme case, as the Al^{3+} is, in fact, the smallest cation which forms this structure at ambient pressures.

The relative magnitudes of the quadrupolar contribution to the total energy are highlighted in table 5. Both the quadrupolar polarization and deformation energies are significantly greater than their dipolar counterparts reflecting the symmetries of the anion sites in both the corundum and bixbyite crystals. Furthermore, the fact that the coordination environment about an anion in the corundum is more distorted away from the ideal tetrahedral than in the bixbyite is reflected in the greater quadrupole contributions to the total energy in the corundum crystal.

Table 5. Cr_2O_3 self and polarization energies in kJ mol^{-1}.

Crystal	$U_{\mathrm{pol,dip}}$	$U_{\mathrm{pol,quad}}$	$U_{\mathrm{self,dip}}$	$U_{\mathrm{self,quad}}$
Corundum	4.3	109.0	2.9	27.0
Bixbyite	1.2	73.3	3.9	13.0

4. Surface relaxation

Surface calculations were performed using the three-dimensional periodic boundary conditions (and the Ewald summation of all coulombic and multipolar interactions) by creating simulation cells containing a pair of matched surfaces separated by a vacuum gap. The surface relaxations were performed in the same manner as for the crystal structure optimization by allowing the ion positions to evolve in molecular dynamics, whilst periodically removing kinetic energy. In order to assess the role of the vacuum gap, surface relaxations were performed for a series of gaps and slab widths. A gap of around 25 a.u. and a slab width of 50.5 a.u. were found to be sufficient to yield converged surface energies (note that this is large compared to that normally used in plane-wave-based *ab initio* methods).

4.1. (0001) surface

Table 6 lists the surfaces energies for the unrelaxed (i.e. a surface created directly by cleaving the relaxed crystal structure) and for the fully relaxed structures of the (0001) surface, compared to the Hartree–Fock values [16] and to previous calculations with a shell model [43]. Also listed are the relaxations obtained from LEED experiments [17]. The fully relaxed *ab initio* surface energy is lower than that from the AIM, whilst the shell model predicts an even lower energy. The relaxed surface energy is considerably smaller than the unrelaxed (as is also the case for *ab initio*), indicative of large surface relaxations or reconstructions. Table 7 lists the percentage changes on relaxation of the first four layers (three Cr^{3+} layers and a single oxide layer). Figure 2 shows a fragment of the corundum crystal, in which it is bounded on the top and bottom by (0001) surfaces and these atomic layers are labelled. The largest relaxations are in the topmost metal cation layer. In the AIM, the separation between this layer and the first oxide layer reduces by around 40% on full relaxation. The LEED experiment [17] also gives an inward surface relaxation of around 40%, consistent with the full AIM analysis. The Hartree–Fock calculation predicts a relaxation of around 50%, whilst the shell model gives an even larger 59% displacement. We will suggest reasons for the discrepancy between the AIM and HF results below. None of the theoretical calculations (including those reported in [17]) support the very large relaxations of the deeper layers inferred from the experimental study.

In order to try to understand the magnitudes of these relaxations, table 7 also lists relaxations for the same Al_2O_3 surface. Here, besides shell model [44] and HF [16] results, density functional results are also available [1, 2]. The shell models and *ab initio* calculations predict a range of values indicating that this relaxation is quite sensitive to the specifics of the interactions — even in an *ab initio* context. The shell model and Hartree–Fock methods predict the same relaxations as for the Cr_2O_3 surface whilst the density functional approach predicts a much larger relaxation, in which the top layer of cations virtually sinks into the top oxide layer.

Table 6. Surface energies and percentage contraction for the first Cr^{3+} layer with respect to the topmost oxide layer for the AIM, compared to a shell model and *ab initio*.

	AIM		HF [16]		Shell [43]
	Unrelaxed	Relaxed	Unrelaxed	Relaxed	Relaxed
0001 U	6.4	4.8	9.36	3.08	1.61
Cr^{3+} relaxation	—	40	—	50	59

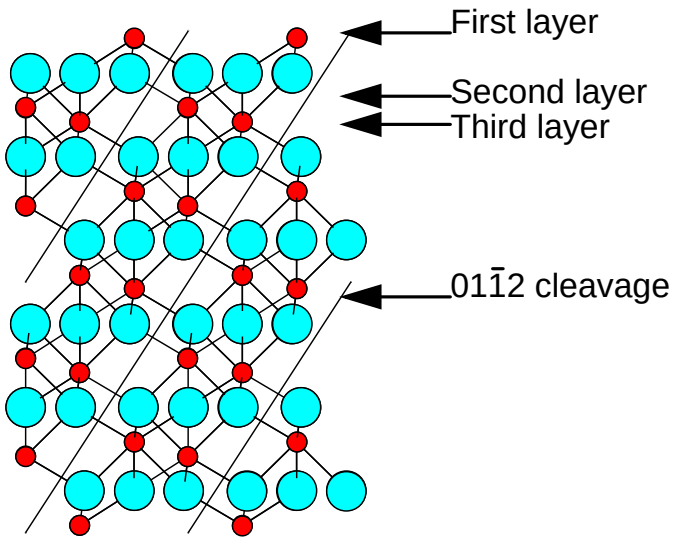

Figure 2. A view of a section of the corundum structure viewed along the *a*-axis. The first three Cr^{3+} layers used in the discussion are indicated, along with a $(01\bar{1}2)$ cleavage plane.

Table 7. Relative relaxations (as percentages) of the first three Cr^{3+} layers for Cr_2O_3 and Al_2O_3.

	Cr_2O_3				Al_2O_3			Al_2O_3/Nb [45]
M^{3+} layer	AIM	HF [16]	Expt. [17]	Shell [43]	Shell [44]	HF [44]	DFT [45]	DFT [45]
1st	−40	−50	−38	−59	−59	−49	−87	+14
2nd	+6	+3	−21	+13	+2	−5	+5	+7
3rd (1st O^{2-})	−30	bulk	+17	+31	—	bulk	+21	+18
3rd (2nd O^{2-})	+11	bulk	+33	bulk	+26	bulk	bulk	bulk

The dominant driving force for the relaxation is the minimization of the long-range coulombic and short-range repulsive interactions. As indicated in figure 2, the unrelaxed surface cation finds itself with a missing layer of anions above it and, hence, it is coulombically attracted to the opposite layer. The magnitude of the relaxation should then be governed by the size of the cation, which determines how far it can 'burrow' into the oxide layer. As a result, one expects the smaller Al^{3+} cation to relax further than Cr^{3+}. These considerations indicate that a relaxation of around 40% for the Cr^{3+} ions is reasonable compared with the 50% for the Al^{3+}, consistent with the experimental outer layer relaxation. Further evidence for this viewpoint comes from the study of Nb monolayers on the oxygen-terminated (0001) surface of Al_2O_3 [45]. This system is equivalent to the pure Cr_2O_3 cation-terminated surface considered here but with the top layer of cations substituted by Nb^{3+}. Table 7 lists the observed relaxations for the density-functional calculations for this system. The presence of a significantly larger cation on the surface ($\sigma_{Nb^{3+}} = 0.86$ Å) results in a relaxation outwards for the top cation layer consistent with the picture of the short-range repulsive forces dominating the coulombic in the unrelaxed geometry.

The relaxation of the lattice perpendicular to the *c*-axis (i.e. parallel to the oxide planes) is much more subtle, as would be expected for an essentially close-packed sublattice. The HF calculations predict a contraction of an oxide triangle about the relaxing surface Cr^{3+} of around

2% whilst the full AIM gives an expansion of about the same magnitude. A relaxation of this magnitude represents a movement of the oxide ions of around 0.03 Å, which is well within the bounds of error in either technique. For example, the AIM predicts an oxide parameter, u_O of 0.286 compared with the experimental value of 0.306, corresponding to more tightly held triangles of oxides about each Cr^{3+}. Assuming that the HF calculations lead to better agreement with experiment (no values are quoted in [16]) then the disagreement in relaxation parallel to the surface is reasonable. The more tightly held triangles of oxides in the AIM tend to be pushed away by the cation as it descends into the topmost layer of oxide anions.

A reason for the quantitative disagreement between the AIM and HF calculations, as regards the size of the outer layer relaxation (40% versus 50%), might be that in the latter all ions below, and including the fourth layer (the third cation layer, cf. figure 2), are fixed in bulk positions. As is clear from table 7, the AIM simulation shows that there are significant relaxations in these layers if the atoms are allowed to move. In order to test the effect of fixing these ions, we have performed the AIM relaxations holding the same ions fixed as in the *ab initio*. Interestingly, this procedure results in an increase in the percentage relaxation of the first cation layer from 40% to around 45%, bringing it closer to the *ab initio* HF result.

The relaxations of the second and third Cr^{3+} layers (table 7) can be understood in terms of the coulombic interactions between the pairs of closest cations which lie across planes of oxides in the *c*-direction. The relatively large relaxation of the third cation layer, for example, can be attributed to the fact that the 'counter-ion' of this cation pair has been removed in the formation of the surface and, as a result, the driving force for its displacement from the centre of the octahedral hole in the corundum structure is lost, so that the third layer cation moves back towards the centre of its hole. Bearing this relaxation in mind, the origin of the larger outermost cation relaxation in the calculations, where the third cation layer is held fixed, becomes clear. In the full calculations, the relaxation of the third Cr^{3+} layer moves this layer closer to the surface so that it tends to repel the outermost cation layer and reduce its inward relaxation.

4.2. ($01\bar{1}2$*) surface*

Figure 2 shows the cleavage planes for the $(01\bar{1}2)$ surface. As a result of the formation of this surface, each Cr^{3+} cation at the surface 'loses' a short Cr–O bond to become five-coordinate with two short and three long Cr–O bonds in the unrelaxed structure. The calculations are performed in a rhombohedral cell of 480 ions.

Again, the energetics and relaxations of the $(01\bar{1}2)$ surface are compared with Hartree–Fock results [18]. Both the unrelaxed and relaxed surface energies (3.30 and 3.05 Jm^{-2} respectively) are slightly higher than the *ab initio* values (2.97 and 2.64 Jm^{-2}) but, in both cases, they are lower than the corresponding relaxed (0001) energy. The change in energies on relaxation are very similar in the two methods. The relaxation of this surface is far more subtle than in the (0001), as indicated by the smaller energy change on relaxation. In terms of the inter-layer separations the HF calculations predict a small ($\simeq 5.5\%$) expansion of the first layer Cr–O separation on relaxation whilst the model predicts a contraction of similar magnitude. Both calculations predict similar magnitude relaxations (of the same sign) for the second layer. These results are very sensitive to the precise nature of the calculation as, for this surface, the unrelaxed separations are themselves very small (0.36 Å and 0.74 Å respectively). As a result, a percentage change of around 5% for the first layer Cr–O separation corresponds to a movement of only 0.018 Å, well within any errors associated with either method. In the HF calculations, for example, magnetism affects length scales by around 0.02 Å [18]. The largest relaxation parallel to the surface involves the shortening of the 'topmost' Cr–O bond.

In the unrelaxed crystal, this bond length is 3.84 a.u. corresponding to one of the three 'long' bonds. On relaxation this bond is shortened by around 0.15 a.u. ($\simeq 4\%$) to a length more in line with the unrelaxed crystalline short bonds (3.76 a.u.). For this surface, unlike the (0001), the relaxations parallel to the surface are of the same magnitude as those perpendicular.

It is interesting to try to explain why the relaxation of the $(01\bar{1}2)$ surface should be so much smaller than that of the (0001), considered above. As was remarked in that discussion, the oxide sublattice is almost close-packed and has little scope for reorganization. The most important factor then becomes the close proximity of pairs of Cr^{3+} ions in the corundum structure which, in the bulk, forces each ion of a pair off the octahedral hole site. As is seen in figure 2, the (0001) cleavage plane cuts through these pairs, so that the top layer Cr^{3+} ion sits above an empty octahedral site, and the repulsion with the nearest-neighbour cation is removed. When relaxation is allowed it moves strongly inwards, towards the empty site. The $(01\bar{1}2)$ cleavage, on the other hand, cuts the crystal through a plane of empty sites, so that the cation pairs involving the surface Cr^{3+} ions are preserved. Except for the loss of one O^{2-} ion from its immediate coordination shell (which is compensated by the small inward relaxation of the remaining oxygens), the surroundings of these ions is thus very similar to that of the bulk crystal, so that there is no driving force for a large-scale reorganization.

The relaxation is small and so the five-coordinate sites remain exposed. Such sites are proposed as important in the adsorption of, for example, CO [20]. Indeed, these five-coordinate sites are similar to those known to be catalytically active on the rutile surfaces of both TiO_2 and SnO_2 [21].

5. Conclusions

The interaction model used in the present work allows for polarization and ion shape changes, and was found to give a good representation of the many-body effects in the alkaline earth oxides, as judged by the comparison of calculated and experimental phonon dispersion curves. *Ab initio* work and such comparisons with experimental information showed that the parameters in the potential transformed sensibly from one system to another, as would be expected for a physically complete interaction model. The parameters of one system could be calculated from those of another by applying scaling factors calculated from the ionic radius and ionic polarizabilities. In the present work, we have extended this potential transformation to Cr_2O_3 and found that, despite the reduction in crystal symmetry which accompanies this change of stoichiometry, the new potential fares very well in comparison with experiment and *ab initio* approaches. In particular, we have shown that the potential works well in predicting surface properties, even though the surface anion site is highly distorted from the high symmetry equilibrium position typical of MO stoichiometry.

The surface calculations highlight one advantage of working with a potential model, rather than performing *ab initio* calculations on a relatively small sample. It would seem that to fully relax the surface, full mobility of a large number of ions must be allowed: significant changes in the relaxation of outer layer atoms are caused by freezing the ionic positions five layers deep.

Acknowledgments

The work was supported by EPSRC through grants GR/L05068 and GR/L49369 and through a CASE studentship (with ICI) to AR. MW is a Royal Society Research Fellow.

References

[1] Manassidis I, DeVita A and Gillan M J 1993 *Surf. Sci. Lett.* **285** L517
[2] Manassidis I and Gillan M J 1994 *J. Am. Ceram. Soc.* **77** 335
[3] Harding J H 1990 *Mol. Sim.* **4** 255
[4] Rowley A J, Ẅemmer P, Wilson M and Madden P A 1998 *J. Chem. Phys.* **108** 10209
[5] Kavanagh D M C, Ryan T A and Mile B 1994 *J. Fluorine Chem.* **64** 167
[6] Neidersen K, Schreier E and Kemnitz E 1997 *J. Catalysis* **167** 210
[7] Farrokhnia A, Sakakini B and Waugh K C 1998 *J. Catalysis* **174** 219
[8] Madden P A and Wilson M 1996 *Chem. Soc. Rev.* **25** 339
[9] Dick B G and Overhauser A W 1958 *Phys. Rev.* **112** 90
[10] Wilson M and Madden P A 1997 *J. Chem. Soc. Faraday Trans.* **106** 339
[11] Wilson M, Madden P A, Pyper N C and Harding J H 1996 *J. Chem. Phys.* **104** 8068
[12] Wilson M and Madden P A 1997 *Molec. Phys.* **90** 75
[13] Rowley A J, Wilson M and Madden P A 1999 in preparation
[14] Wilson M, Exner M, Huang Y and Finnis M W 1996 *Phys. Rev.* B **54** 15683
[15] Gale J D, Catlow C R A and Mackrodt W C 1992 *Modelling Simul. Mater. Sci. Eng.* **1** 73
[16] Rehbein C, Harrison N M and Wande A 1996 *Phys. Rev.* B **54** 14066
[17] Rohr F, Bäumer M, Freund H-J, Mejias J A, Staemmler V, Müller S, Hammer L and Heinz K 1997 *Surf. Sci.* **372** L291
[18] Rehbein C, Harrison N M and Wande A 1998 *Surf. Rev. Lett.* **5** 337
[19] Schröder S L M, Moggridge G D, Rayment T and Lambert R M 1997 *J. Physique* **7** 923
[20] Scarano D, Zecchina A, Bordiga S, Ricchiardi G and Spoto G 1993 *Chem. Phys.* **177** 547
[21] Henrich V E 1985 *Rep. Prog. Phys.* **48** 1481
[22] Henrich V E and Cox P A 1994 *The Surface Science of Metal Oxides* (Cambridge: Cambridge University Press)
[23] McKay J M and Henrich V E 1984 *Surf. Sci.* **137** 463
[24] Cynn H, Isaak D G, Cohen R E, Nicol M F and Anderson O L 1990 *Am. Mineral.* **75** 439
[25] Marton F C and Cohen R E 1994 *Am. Mineral.* **79** 789
[26] Wilson M 1998 *J. Am. Ceram. Soc.* **81** 2558
[27] Shannon R D 1976 *Acta. Crystallogr.* A **32** 751
[28] Wilson M and Madden P A 1993 *J. Phys.: Condens. Matter* **5** 2687
Wilson M, Costa-Cabral B J and Madden P A 1996 *J. Phys. Chem.* **100** 1227
Foley M F, Wilson M and Madden P A 1995 *Phil. Mag.* B **71** 557
[29] Lewis G V and Catlow C R A 1985 *J. Phys. C: Sol. State Phys* **18** 1149
[30] Wilson M, Madden P A, Ẅemmer P and Fowler P W 1999 *J. Chem. Phys.* submitted
[31] Lide D R 1994 *CRC Handbook of Chemistry and Physics* (Boca Raton, FL: CRC press)
[32] Pyper N C 1991 *Adv. Sol. State Chem.* **2** 223
[33] Fowler P W and Madden P A 1985 *Phys. Rev.* B **31** 5443
[34] Kelly H M and Fowler P W 1993 *Mol. Phys.* **80** 135
[35] Ẅemmer P, Fowler P W, Wilson M and Madden P A 1998 *J. Phys. Chem.* A **102** 8377
[36] Tang K T and Toennies J P 1984 *J. Chem. Phys.* **80** 3726
[37] Slater J C and Kirkwood J G 1931 *Phys. Rev.* **37** 682
[38] Starkschall G and Gordon R G 1972 *J. Chem. Phys.* **56** 2801
[39] Harding J H and Pyper N C 1995 *Phil. Mag. Lett.* **71** 113
[40] Wyckoff R W G 1965 *Crystal Structures* (New York: Interscience)
[41] Lee W E and Lagerlof K P D 1985 *J. Electron Microsc. Tech.* **2** 247
[42] Wells A F 1984 *Structural Inorganic Chemistry* 5th edn (Oxford: Clarendon)
[43] Lawrence P J, Parker S C and Tasker P W 1988 *Commun. Am. Ceram. Soc.* **71** 389
[44] Mackrodt W C 1992 *Phil. Trans. R. Soc.* A **341** 301
[45] Kruse C, Finnis M W, Lin J S, Payne M C, Milman V Y, DeVita A and Gillan M J 1996 *Phil. Mag. Lett.* **73** 377